JNeurosci
THE JOURNAL OF NEUROSCIENCE

Research Articles: Systems/Circuits

Cochlear efferent innervation is sparse in humans and decreases with age

https://doi.org/10.1523/JNEUROSCI.3004-18.2019

Cite as: J. Neurosci 2019; 10.1523/JNEUROSCI.3004-18.2019

Received: 28 November 2018
Revised: 27 September 2019
Accepted: 5 October 2019

Cochlear efferent innervation is sparse in humans and decreases with age

Liberman LD[1] and Liberman MC[1,2]

Abbreviated Title: Cochlear efferents in aging humans

[1]Eaton-Peabody Laboratories, Massachusetts Eye and Ear, Boston, MA 02114
[2]Department of Otolaryngology, Harvard Medical School, Boston, MA 02115

Page Count: 23 including Figure Captions
Figures: 10
Abstract: 175 words
Introduction: 585 words
Discussion: 1471 words (without in-text citations)

Conflicts and Disclosures: The authors have no conflicts of interest or financial relationships to disclose

Corresponding author:

M. Charles Liberman, Ph.D.
Eaton-Peabody Laboratories
Massachusetts Eye and Ear Infirmary,
243 Charles St., Boston, MA 02114-3096, USA.
Tel: 617-573-4233
E-mail: Charles_Liberman@meei.harvard.edu

Abstract

The mammalian cochlea is innervated by two cholinergic feedback systems called the medial (M) and lateral (L) olivocochlear (OC) pathways, which send control signals from the brainstem back to the outer hair cells and auditory-nerve fibers, respectively. Despite countless studies of the cochlear projections of these efferent fibers in animal models, comparable data for humans is almost completely lacking. Here, we immunostained the cochlear sensory epithelium from 23 normal-aging humans (14 males and 9 females), aged 0 – 86 years, with cholinergic markers to quantify the normal density of MOC and LOC projections, and the degree of age-related degeneration. In younger ears, the MOC density peaks in mid-cochlear regions, and falls off both apically and basally, whereas the LOC innervation peaks near the apex. In older ears, MOC density decreases dramatically, whereas the LOC density does not. The loss of MOC feedback may contribute to the age-related decrease in word-recognition in noise, however, even at its peak, the MOC density is lower than in other mammals, suggesting the MOC pathway is less important for human hearing.

Significance Statement

The cochlear epithelium and its sensory innervation are modulated by the olivococochlear (OC) efferent pathway. Although the medial (M)OC reflex has been extensively studied in humans, via contralateral-sound suppression, the cochlear projections of these cholinergic neurons have not been described in human. Here, we use immunostaining to quantify the MOC projections to outer hair cells and lateral (L)OC projections to the inner hair cell area in humans aged 0 to 89 yrs. We show age-related loss of MOC, but not LOC innervation, which likely contributes to hearing impairments, and a relative paucity of MOC terminals at all ages, which may account for the relative weakness of the human MOC reflex and the difficulty demonstrating a robust functional role in human experiments.

Introduction

The vertebrate inner ear is modulated by cholinergic feedback from the brainstem via the olivocochlear (OC) efferent pathway (Guinan, 2010). The OC system in mammals comprises a few thousand neurons, divided into medial (M) and lateral (L) subdivisions, based on cell-body location in the superior olivary complex (Guinan et al., 1983; Guinan et al., 1984). MOC neurons are myelinated and represent the effector arm of a sound-evoked negative-feedback loop (Liberman and Brown, 1986) that projects to cochlear outer hair cells (OHCs), as schematized in Figure 1. MOC activity diminishes cochlear sensitivity (Wiederhold and Kiang, 1970) by reducing the normal contribution of OHC electromotility to amplification of mechanical vibration of the sensory epithelium (Russell and Muragasu, 1997). The LOC neurons are ummyelinated and project to dendrites of auditory nerve fibers (Figure 1) near their synapses with inner hair cells (IHCs) (Liberman, 1980), where they modulate the excitability of these sensory neurons (Groff and Liberman, 2003). It is not clear whether LOC neurons are activated (or suppressed) by sound.

Several functional role(s) have been suggested for these feedback systems. MOC feedback extends the ear's dynamic range and increases detectability of signals in noise (Kawase et al., 1993). The LOC system balances neural outputs from the two ears, as needed for localization of high-frequency sounds based on interaural level differences (Darrow et al., 2006). Both MOC and LOC systems protect the ear from acoustic overstimulation (Rajan, 1988; Kujawa and Liberman, 1997; Darrow et al., 2007), and both are necessary for normal cochlear development (Walsh et al., 1998).

Neuroanatomy, neurophysiology, synaptic transmission and peripheral effects of MOC and LOC systems have been extensively studied in animals (Guinan, 2010). However, in humans, only the peripheral effects of the MOC system have been well characterized. Because the MOC reflex is binaural, contralateral sound can activate MOC fibers to the ipsilateral ear and suppress responses such as

otoacoustic emissions (Collet et al., 1990). Studies of "contra-sound suppression" suggest that MOC reflex strength declines with age (Kim et al., 2002; Jacobson et al., 2003; Konomi et al., 2014; Lisowska et al., 2014). Given the hypothesized role in the control of masking, this reflex decline may contribute to problems hearing-in-noise in the aging ear. However, based on the contra-sound suppression assay, the MOC reflex in humans is significantly weaker than in other laboratory mammals, e.g. mice (Chambers et al., 2012).

In humans, understanding of OC neuroanatomy is fragmentary. The organization of LOC vs. MOC subdivisions in the brainstem has been verified (Moore et al., 1999), and the presence of cholinergic fibers and terminals in the cochlea has been documented (Ishii et al., 1967; Nomura, 1976; Schrott-Fischer et al., 1994; Schrott-Fischer et al., 2007). Electron-microscopic studies show cochlear efferent synapses that resemble those in animals (Nadol, 1983a, b). However, no study has quantified the normal density of efferent innervation along the cochlear frequency (spiral) axis, or the age-related changes in these projections.

Here we address these fundamental issues with a quantitative confocal study of immunostained inner ears from 23 "normal-aging" subjects, i.e. individuals without exposure to known ototoxic substances or excessive noise exposure, ranging in age from a few weeks to 86 years. Results show different frequency distributions for LOC vs. MOC projections in the younger ears, and an age-related loss of MOC innervation, without loss of LOC projections. Results also suggest that the MOC innervation is relatively sparse in humans compared to mouse, guinea pig and rhesus macaque, which helps explain why the human MOC reflex is so weak compared to other mammals studied.

Methods

Subjects and Groups: The materials for the present study are human temporal bones obtained at autopsy. The subject pool included 23 ears from 23 individuals, ranging in age from neonatal to 86 yrs. The majority (21/23) were also studied in a prior report on age-related primary degeneration of auditory-nerve fibers (Wu et al., 2018). None of these cases had any explicit history of otologic disease other than age-related hearing loss, which was noted in the medical record for three cases, aged 78, 80 and 86. Two of these three cases had audiograms: both showed thresholds within 10 dB of the median better-ear threshold for age- and gender-matched subjects (Gordon-Salant, 2005). One of the youngest subjects (age 24) had an audiogram documenting normal thresholds at all standard frequencies. All procedures concerning the handling of human tissues were approved by the Human Studies Committee of the Massachusetts Eye and Ear. For comparison of the density of efferent innervation, four ears from each of three other species (mouse, guinea pig and rhesus macaque) were also processed and imaged in identical fashion. Mice were male CBA/CaJ mice (6.5 wks), guinea pigs were male and female Hartley strain (6.5 wks), and monkeys were male (9.5 and 11.5 yrs). Mouse and guinea pig tissue was extracted at the Massachusetts Eye and Ear under protocols approved by the institutional Animal Care Committee. Rhesus tissue was extracted at Vanderbilt University under protocols led by Dr. Ram Ramachandran and approved by his institutional Animal Care and Use Committee.

Cochlear Processing: The human temporal bones were extracted with a bone-plugging tool (Schuknecht, 1993), from 5 – 13 hrs after death (median = 9.0) and immersed in buffered 10% formalin; round and oval windows were opened and formalin flushed through the scalae. After post-fixation (4°C) for ≥ 6 days, the bone plug containing the cochlea was drilled to remove much of the petrous bone, and then immersed in decalcifying solution (EDTA) at room temperature for ~4 wks. Cochleas from mice, guinea pigs and monkeys were fixed by intravascular and cochlear perfusion of buffered 4% paraformaldehyde, and then postfixed for 2 hrs. Cochleas were microdissected into 6-12 pieces (depending on species), each containing the osseous spiral lamina and the attached organ of Corti. Following immunostaining, the cochlear spiral was mapped onto low-power images of the microdissected pieces by tracing an arc along the tunnel of Corti, after which, normalized cochlear length was converted to frequency. For humans, this conversion was based on a Greenwood function (Greenwood, 1990)

modified to produce best frequencies at the apex and base of the cochlea of 100 Hz and 20 kHz, respectively. Cochlear frequency maps for mouse (Taberner and Liberman, 2005), guinea pig (Tsuji and Liberman, 1997) and monkey (Valero et al., 2017) are described elsewhere. In humans, fourteen frequency locations from 0.175 to 16 kHz were calculated, and superimposed on the low-power images of the microdissected pieces, at half-octave intervals along the length of the spiral, to pinpoint the image-acquisition loci in each case. In each of the other species, images were also acquired at several log-spaced frequency locations.

Immunostaining Protocols: Cochlear pieces were permeabilized with a freeze/thaw step in 30% sucrose, followed by 1 hr at room temperature in a blocking buffer (PBS with 5% normal horse serum and 0.3 - 1% Triton X-100). Tissue was then incubated overnight at 37 ºC with some combination of the following primary antibodies (plus 0.3 – 1% TritonX): 1) chicken anti-neurofilament (Chemicon #AB5539) at 1:1000 to visualize nerve axons, 2) rabbit anti-Myosin VI and/or VIIa (Proteus Biosciences #25-6791 and 25-6790, respectively) at 1:100 to count hair cells and 3) goat anti-ChAT (choline acetyltransferase; Millipore #AB144P) at 1:100 to quantify efferent projections from the olivocochlear bundle. Primary incubations were followed by 2 sequential 60-min incubations at 37°C in species-appropriate secondary antibodies (coupled to Alexafluor dyes) with 0.3 - 1% TritonX. After immunostaining, all pieces from each cochlea were slide-mounted in Vectashield, coverslipped, and the coverslip sealed with nail polish. After analysis of hair cells and efferent terminals, the coverslips were removed and the tissue was incubated in a fluorescent membrane dye (CellMask® Orange, Thermo Fisher #C10045) at 1:5000 with 0.3% TritonX for 5 minutes to label the myelin sheaths. The pieces were re-mounted and coverslipped with Vectashield. This final treatment did not disturb the pre-existing immunostains.

Hair Cell counts: For all stained tissues, confocal z-stacks were acquired at equally spaced locations along the spiral, with 0.33 μm z-spacing on a Leica SP8 using a 63x glycerol objective (1.3 N.A.). At each cochlear location, an image stack of IHCs and OHCs spanning ~250 μm of cochlear length was acquired. In each stack, hair cell fractional survival was quantified by counting the number of remaining cells in each row as the numerator and estimating the number of missing cells to include in the denominator. In cases with only scattered loss, missing cells are easy to count as gaps in the regular array. In cases with more massive losses, the denominator was estimated from the minimal-loss cases, using mean values as a function of cochlear location. Among the OHCs, the denominator was set by the 1st row cells, because they are always the most regularly arrayed.

Innervation Analysis: To estimate the innervation density of the lateral olivocochlear (LOC) and medial olivocochlear (MOC) projections, we acquired high-power images of the inner and outer hair cell area, respectively. In each cochlear location, and separately for inner and outer hair cell areas, we acquired 2 adjacent z-stacks (each spanning 112 μm of the cochlear spiral), taking care to span, along the z axis, the entire region containing ChAT positive terminals or fibers. The ChAT channel of each z-stack maximum projection was extracted and ported to ImageJ, where the default auto-thresholding algorithm was used to count the total signal in the projection (https://imagej.net/Auto_Threshold#Default), expressed as the number of suprathreshold pixels. This algorithm requires no user input: it divides the entire image into object vs. background by taking an initial threshold, computing averages of the pixel values ≥ threshold and those < threshold; then incrementing the threshold value until it is larger than the composite average.

In prior studies, we have compared several alternate approaches to the quantification of MOC innervation density, i.e. counting of tunnel-crossing fascicles or measuring their summed diameter (Liberman and Gao, 1995; Liberman et al., 2000), counting the average number of MOC terminals contacting each OHC (Liberman et al., 1990; Liberman et al., 2014), or measuring the projected silhouette areas, either manually (Maison et al., 2003) or automatically (Yin et al., 2014). In prior work, we have shown 1) that the fascicle diameters in the tunnel are highly correlated with silhouette areas of terminals under the OHCs (Liberman and Gao, 1995), 2) that immunostained silhouettes are highly correlated with maximum terminal areas extracted from serial-section electron microscopy (Liberman et al., 1990), and 3) that terminal counts are highly correlated with silhouette areas (Liberman unpublished). Here, we chose

to use automatic measurement of immunostained silhouette areas, 1) because it is completely computer driven and thus not subject to user bias, and 2) because so many of the MOC terminals were small *en passant* swellings, it was difficult to set a reproducible criterion for their enumeration.

Experimental Design and Statistical Analysis: This was a prospective study of autopsy cases of either sex from the Massachusetts General Hospital, meeting the following inclusion criteria: temporal bones were extracted at a post-mortem time < 13 hrs and there was no medical history of otological disease. Statistical analysis was carried out in GraphPad Prism v8.2.1. Age-related changes (Figs. 2A, 5A, 7A and 9B) were assessed by linear regression, and intergroup comparisons (Figs. 2B&C, 5B&C and 7B&C) were assessed by two-way ANOVA followed by a Holm-Sidak multiple comparisons test.

Results

A. Age-related loss of Hair Cells

The human cochlea contains a sensory epithelium, the organ of Corti (Figure 1), that spirals for ~35 mm from the high-frequency basal tip to the low-frequency apex. This epithelium normally contains one row of roughly 3500 inner hair cells (IHCs), three rows each containing about 4200 outer hair cells (OHCs), and an occasional 4th row of OHCs. For each of the 23 temporal bones in the present study, the sensory epithelium was microdissected and immunostained. Hair cell counts and analysis of the afferent and efferent innervation was carried out on confocal z-stacks corresponding to half-octave intervals of cochlear frequency from 0.175 to 16 kHz. The fractional survival of hair cells is summarized in Figure 2. Age-related loss of OHCs outpaces the age-related loss of IHCs by more than 2:1 (Figure 2A): 4.5% loss per decade for OHCs vs. 2.0% loss per decade for IHCs. Although, with increasing age, scattered hair cell loss is seen throughout the cochlear spiral for both IHCs and OHCs, the loss is most dramatic for IHCs in the extreme base (Figure 2B) and in both the basal and apical extremes among the OHCs (Figure 2C).

B. MOC innervation and age-related loss

Medial olivocochlear (MOC) neurons in mammals project from cell bodies in brainstem regions near the medial superior olive, and send myelinated axons to the OHC region, both ipsilaterally and contralaterally, where they terminate on the OHCs (Figure 1), as well as on the spiraling dendrites of the OHCs' sensory (afferent) innervation, the type-II spiral ganglion neurons (Liberman and Brown, 1986; Thiers et al., 2002).

Since the MOC system is predominately cholinergic, those projection patterns are well seen in the distribution of ChAT-immunostained fibers and boutons in the osseous spiral lamina (Figure 3) and organ of Corti (Figure 4). In the osseous spiral lamina, efferent fibers take a spiral course within a series of bundles traveling orthogonally to the radially oriented auditory-nerve fibers, riding on the scala-vestibuli side of the sensory fascicles (Figure 3, zy projections). As they approach the organ of Corti, the efferents turn radially to join the afferents. In this region, which is close to the distal ends of these fibers in the organ of Corti, very few of the ChAT-positive efferents appear myelinated, i.e. surrounded by a Cellmask-positive sheath (Figure 3A,B xz projections).

The MOC terminal boutons in the organ of Corti (Figure 4) are especially well seen in the re-projection of the image stacks into the zy plane (Figure 4A,C), where the sensory epithelium is viewed as if in a thick cross-section. MOC boutons (white-filled arrows), can be seen on the basal pole and along the sides of the hair cells (stained with anti-myosin VIIa; red) as well as among the type-II dendrites (stained with anti-neurofilament; blue), which spiral between the supporting cells in the region underneath the OHCs, as shown by the black-filled arrow in Figures 3A,C. A radial gradient is suggested by the images in Figure 4, i.e. the innervation density is highest among the 1st-row OHCs and lowest among the 3rd-and 4th-row OHCs. An age-related loss of MOC innervation density is suggested by the difference in the numbers of ChAT-positive boutons in 4.0 kHz region of the 78 yr-old subject (Figure 4C,D) compared with the same region in the 39 yr-old subject (Figure 4A,B).

To quantify the density of MOC innervation as function of cochlear location and age, we took confocal xy projections, like those in Figures 4B and 4D, extracted the ChAT channel, applied an auto-thresholding algorithm in ImageJ, and averaged the resultant total silhouette area in each projection across cases, and at each cochlear location. Several important trends are visible in the results, as summarized in Figure 5.

First, in the youngest ears (0 – 40 yrs, Figure 5B), the density peaks in the 4-kHz region (upper basal turn) and falls off slowly towards the apex, and more rapidly towards the base. A similar pattern, i.e. peak density occurring in the upper basal turn of the cochlea, has been observed in other low-frequency mammals such as cat and guinea pig (Liberman et al., 1990; Liberman and Gao, 1995).

Secondly, the MOC density decreases with age. When data from each case are averaged across all audiometric frequencies (0.25 – 8.0 kHz inclusive) and plotted vs. age (Figure 5A), the linear regression is highly significant (r^2 =0.45, p = 0.0005). The age-related differences are greatest in the high-frequency regions (Figure 5B), where the mean MOC areas in the oldest group are less than half of those in the youngest group. Two-way ANOVAs suggest significant pairwise differences between all groups: young vs. middle, p = 0.36; young vs. old, p < 0.0001; middle vs old, p < 0.0001.

Lastly, the age-related loss of MOC density is not simply due to the age-related loss of peripheral targets, i.e. OHCs. As shown in Figure 5C, the age-related loss of MOC terminals in is still significant when the density is normalized to the numbers of surviving OHCs in the same z-stacks: p = 0.0002 for young vs. old groups and p < 0.0001 for middle vs. old groups (young vs. middle are statistically indistinguishable: p = 0.60).

C. LOC innervation and age-related loss

LOC neurons in the mammal project via unmyelinated axons from the region in and/or around the lateral superior olive, primarily to the ipsilateral cochlea. Throughout much of their course from brainstem to cochlea, they are intermingled with MOC axons, including in the spiraling bundles within the osseous spiral lamina (Figure 3). Within the organ of Corti, each peripheral LOC axon continues to spiral in the inner spiral bundle, directly underneath the IHCs, and/or in the tunnel spiral bundle (TSB) (Figure 1). As they spiral, they send off terminal branches and make *en passant* synapses with their peripheral targets. These targets include 1) primarily the unmyelinated terminals of (afferent) auditory-nerve fibers innervating IHCs, as well as 2) the IHCs themselves, 3) the afferent auditory-nerve fibers contacting OHCs and 4) the MOC fibers as they pass through the tunnel spiral bundle on their way to the OHCs (Liberman, 1980).

As suggested by the confocal images in Figure 6, there is an apical-basal gradient of innervation density for the LOC system. These trends were quantified by measuring silhouette areas in the ChAT channel, exactly as for the MOC system. As shown in Figure 7B, the peak density for all age groups is at a much more apical (lower frequency) cochlear locus than the MOC system (Figure 5). The age-related changes were less dramatic than for the MOC system: the relation between age and LOC density, as averaged across all audiometric frequencies, was borderline significant (Figure 7B; p = 0.04). When considering the apical-basal LOC distributions (Figure 7B), all the age groups were statistically indistinguishable: young vs. middle, p = 0.85; young vs. old, p = 0.10; middle vs. old, p = 0.051. After adjusting for the age-related loss of IHCs (Figure 2A), and thus, by extension, for the loss of their peripheral targets (the auditory-nerve fibers), intergroup differences still were not significant (Figure 7C): young vs. middle, p = 0.77; young vs. old, p = 0.62; middle vs. old, p = 0.79.

D. Interspecies Comparisons of MOC and LOC projections

Qualitative comparison to prior cholinergic immunostaining studies of cochleas from cat (Liberman et al., 1990), mouse (Liberman et al., 2014), guinea pig (Liberman and Gao, 1995) or ferret (Irving et al., 2011) suggest that the MOC system is less robust in humans than in other well-studied laboratory

animals. To make the comparison more quantitative, we prepared new material from mouse, guinea pig and rhesus macaque, using the same antibodies and the same data-analysis techniques as were applied to the human ears. In Figure 8, we compare confocal images from the region of maximum MOC density in a human cochlea, to those from the other three species. The 1st-row OHCs in each stack, as traced from the Myosin VIIa channel, are superimposed for comparison. In the mouse and guinea pig, the regular OHC array is easily discernable from the ChAT channel, because almost every OHC has from 2 – 4 ChAT-positive terminals contacting it. A radial MOC gradient is clear in the guinea pig: the 1st row is more heavily innervated than the 2nd row and the 2nd is more heavily innervated than the 3rd. In rhesus, the radial gradient is stronger, in that some OHCs in the 2nd row, and many in the 3rd, are not contacted by any MOC terminals. In human, the innervation appears the patchiest: i.e. many cells in the 2nd and 3rd row appear uninnervated. Note also that ChAT-positive, tunnel-crossing fibers (arrowheads in Figure 8) are roughly half as numerous in the human as in the other species: human, 8 fibers for 13 1st-row OHCs; rhesus, 15 fibers for 15 OHCs; guinea pig, 13 fibers for 14 OHCs; mouse, 17 fibers for 16 OHCs.

Quantitative comparison of MOC silhouette areas from the peak-density region, normalized to the number of OHCs contacted, yields the following mean values for μm^2/OHC (±SEMs): guinea pigs, 34.7 (±0.7) at the 4-kHz region; monkeys, 21.9 (±1.3) at 2 kHz; humans, 17.3 (±0.7) at 2 kHz; and mice,13.6 (±0.6) at 22.6 kHz. By this metric, the peak human projection is 50% of that in guinea pig and 80% of the rhesus, but slightly larger than the mouse. However, this absolute-size metric ignores the enormous size difference of the OHCs they are driving: in the peak MOC regions, mouse OHCs are 4.8 μm in diameter and 25.6 μm tall, for a surface area of 387 μm^2, whereas human OHCs are 7.8 μm in diameter and 38.2 mm tall, for a surface area of 986 μm^2. In Figure 9A, we plot the mean MOC terminal areas, expressed as percentage of these species- and place-appropriate OHC-area metrics. By this measure, the peak human MOC projection is less than half as large as that in any of the other three species. To address the possibility that the reduced MOC innervation is an artifact of post-mortem autolysis, we regressed the MOC silhouette areas against post-mortem time and saw no significant correlation ($r^2 = 0.0024$, $p = 0.82$; data not shown).

Evidence that MOC silhouette areas, as measured here, are functionally significant comes from multiple sources. In cats, MOC silhouette areas vs. cochlear frequency, extracted from synaptophysin-immunostained cochleas, are very similar to MOC-elicited threshold elevations in auditory-nerve fibers plotted vs. their best frequencies [Figure 18 in (Liberman et al., 1990)]. In mouse, counts of surviving MOC terminals after de-efferentation surgery are highly correlated with MOC effect size in the same ears [$r^2 = 0.58$, $p < 0.0001$ (Liberman et al., 2014)], measured as the cochlear threshold elevation elicited by electrical stimulation of the MOC bundle. Here, we re-analyzed those mouse data, measuring MOC silhouette areas instead of terminal counts, and found that the correlations were just as significant (Figure 9B, $r^2 = 0.56$, $p < 0.0001$). Not surprisingly, the terminal counts and the silhouette areas were also highly correlated: $r^2 = 0.87$, $p < 0.0001$ (data not shown).

Qualitative comparison of LOC innervation densities does not suggest any striking interspecies differences. Figure 10 compares regions of maximum innervation density in human vs. mouse. If anything, the human LOC is denser than that in the mouse; for example, the tunnel spiral bundle (TSB in Figure 10) is better developed in the human. No quantitative interspecies comparisons were undertaken, because the functional significance of this unmyelinated system is much more poorly understood, and because the peripheral targets, the unmyelinated terminals of auditory-nerve fibers are too small to be well resolved in these confocal z-stacks, thus no meaningful interspecies normalization to adjust for size differences is possible.

Discussion

A. OC effects at low vs. high frequencies

All vertebrate hair cell systems, including those in cochlear, vestibular and lateral-line epithelia, are modulated by a neuronal efferent pathway that projects either to the hair cells themselves or the sensory

neurons contacting them (Klinke and Galley, 1974). Although such feedback may be important to several aspects of sensory processing, a common functional role appears to be an automatic gain control, to adjust the dynamic range of the sensor according to the overall level of the stimulus (Guinan, 2010).

Activation of MOC terminals in mammals elevates cochlear thresholds by decreasing intracellular receptor potentials and thereby decreasing the reverse transduction of those electrical signals into mechanical motion, as effected by the motor protein, prestin, in OHC membranes (Fuchs and Lauer, 2019). As in other "low-frequency" mammals (Liberman and Gao, 1995; Liberman et al., 2000), the density of MOC terminals peaks in the upper basal turn, around 2 - 4 kHz in our youngest subjects (Figure 5), suggesting that this sound-evoked negative feedback is most important for high-frequency stimuli. Similarly, in cats and guinea pigs, MOC innervation peaks in the 5 - 10 kHz region (Liberman et al., 1990; Liberman and Gao, 1995). Correspondingly, when MOC activity is evoked by electrically stimulating the OC bundle, maximum effects on cochlear thresholds are also seen for fibers tuned to frequencies from 5 - 10 kHz in cats (Guinan and Gifford, 1988).

Such a high-frequency bias is consistent with a functional role of MOC feedback in the control of noise masking, especially at high frequencies (Kawase et al., 1993). One of the mechanisms underlying the decreasing response in the auditory nerve to a transient signal in the presence of continuous noise is vesicle depletion at the IHC synapse (Delgutte, 1990). Since the MOC reflex has an onset time constant of >100 msec (Warren and Liberman, 1989; Backus and Guinan, 2006), the MOC's negative feedback can enhance the auditory-nerve response to a stimulus transient (Winslow and Sachs, 1987) by suppressing the tonic response to, and synaptic fatigue from, a continuous noise. This is particularly important at high frequencies (> 1 kHz), where there is diminished ability of auditory-nerve fibers to phase-lock to the incoming stimulus (Johnson, 1980), which can provide alternate cues about the stimulus when the signal-to-noise ratio is poor.

In animals and humans, the MOC reflex can be evoked by sound in either ear. Thus, its strength can be assessed by measuring elevation of ipsilateral thresholds by a contralateral sound (Liberman, 1989). Contralateral-sound suppression in humans typically peaks for ipsilateral frequencies $\leq$ 1 kHz (Kim et al., 2002; Lilaonitkul and Guinan, 2012), which is 1 – 2 octaves lower than the MOC innervation peak (Figure 5). Similarly, in cats, contralateral-sound suppression peaks near 2 kHz (Liberman, 1991), which is 2 octaves lower than the peak MOC density (Liberman et al., 1990) or the peak in shock-evoked threshold elevations (Guinan and Gifford, 1988). In animals, this discrepancy has been ascribed to an anesthesia-related decrease in sound-evoked responses of high-frequency MOC fibers (Liberman, 1988). Since the human assays are performed without anesthesia, an alternative explanation is needed. Perhaps the submaximal reflex activation of MOC neurons at the peak innervation region arises because full activation of this higher frequency "hot spot" requires descending control from higher centers, superimposed on the brainstem reflex (Suthakar and Ryugo, 2017), which might not be activated under the passive listening conditions present during routine testing of MOC reflexes in humans.

With respect to the LOC innervation, less is known about the apical-basal gradient in other mammals. In cat, LOC terminal density is roughly constant from apex to base, as seen by injection of radioactive tracers into the lateral superior olive (Guinan et al., 1984)). In mouse, cholinergic markers in the IHC area show a relatively uniform projection with a very broad peak in roughly the middle of the cochlea (Maison et al., 2003). Both appear fundamentally different from the human pattern, which shows a strongly decreasing gradient from apex to base (Figure 7B). Since the peripheral effects of LOC terminals are more diffuse, difficult to evoke, and more poorly understood (Groff and Liberman, 2003), it is impossible to compare the morphological gradients to any observed physiological gradients.

B. OC effects in humans vs. other mammals

The MOC projections we observed in human ears seemed qualitatively less robust than in other common experimental mammals, e.g. guinea pigs (Burgess et al., 1997), cats (Liberman et al., 1990), ferrets (Irving et al., 2011) or mice (Liberman et al., 2014). As shown in Figure 8, in mouse or guinea

pig, every OHC in all three rows is innervated by multiple MOC terminals. In human, by contrast, few OHCs have multiple MOC contacts, and some have none, especially in the third row. Furthermore, the orthogonal views (Figure 4A) show that many ChAT-positive terminals in humans are below the basal pole of the OHC, where they synapse on type-II afferent fibers, as is well described in ultrastructural studies of human cochleas (Thiers et al., 2002).

Our quantitative analysis (Figure 9A) corroborates the qualitative impression: i.e. when normalized to the sizes of the OHCs they contact, peak MOC innervation in human is ~50% of that in mouse or rhesus and < 40% of that in guinea pig. Such a normalization seems reasonable, as a rough approximation, given that MOC functional effects are mediated via OHC transmembrane voltage, as generated by opening of calcium-activated K^+ channels. Thus, any MOC-mediated voltage changes in the OHC will be inversely proportional to the cell's capacitance, which, in turn, will be proportional to surface area.

These morphological observations suggest that MOC feedback in humans is weaker than in other mammals. Indeed, in normal young adults, OC activation by a moderate-level contralateral sound attenuates ipsilateral probe responses by only 1-2 dB (Collet et al., 1990; Kim et al., 2002; Chambers et al., 2012; Abdala et al., 2014). In contrast, in an unanesthetized mouse, contralateral-sound suppression is ~10 dB (Chambers et al., 2012), and in an unanesthetized guinea pig, ipsilaterally evoked MOC suppression is close to 20 dB (Boyev et al., 2002). Similarly, in anesthetized cats, electrical stimulation of the MOC system can elevate auditory-nerve thresholds by ~20 dB (Guinan and Gifford, 1988).

Correspondingly, human studies designed to reveal MOC effects on auditory performance have yielded relatively small effects (for review, see (Guinan, 2010)). One particularly well-controlled study compared hearing-in-noise performance in one ear, with vs. without an OC elicitor in the contralateral ear. OC activation made only a small improvement (10-15%) on a phoneme identification task in normal subjects. Importantly, this contralateral-sound enhancement was absent in five subjects that had undergone an VIIth nerve surgery for intractable vertigo that should cut the OC bundle without disturbing the auditory nerve (Giraud et al., 1997).

In contrast to the sparsity of MOC projections *re* other mammals, the LOC projection in humans seemed comparably robust, as illustrated by the mouse-human comparison in Figure 10. In both species, the LOC terminals form a cluster that appears to cover the basal pole of the IHCs. The major difference is the prominence of the tunnel spiral bundle in humans, which suggests that LOC fibers may spiral for longer distances in the human than in mouse. The robustness of the LOC projection in our human material helps to argue against the idea that the paucity of MOC projections is an artifact of post-mortem autolysis of ChAT immunoreactivity.

C. Aging and the OC system

In a prior report on the same human ears studied here, we showed a significant age-related loss of the myelinated "type-I" sensory fibers innervating IHCs, without a significant age-related loss of the unmyelinated type-II afferents innervating OHCs (Wu et al., 2018). Here, we saw parallel patterns in the age-related degeneration of OC projections, i.e. a significant loss of the myelinated MOC pathway, and minimal age-related loss of the unmyelinated LOC pathway. Furthermore, the slope of the age-related MOC decline (7.0% per decade) was similar to that of the age-related type-I decline (7.8% per decade). The reasons for a difference in age-related loss of myelinated vs. unmyelinated fibers is unclear, however the myelinated type-I fibers are also more vulnerable than unmyelinated type-IIs to other insults such as acoustic trauma or surgical transection of the central axons (Spoendlin, 1975, 1979).

There have been few studies of the age-related decline in the magnitude of MOC reflex strength in humans, especially within the age range for most of our subjects (50 – 90). However, two studies that include a group over 50 yrs report a significant decrease in MOC strength, especially at higher frequencies, i.e. 4 kHz vs 1 kHz probe tones (Kim et al., 2002; Lisowska et al., 2014). These results are consistent with the degeneration patterns we observed for MOC innervation density, which also show larger effect in the 4-kHz cochlear region than the 1 kHz region (Figure 5). One study reports increased

contra-sound effects in a group of older subjects (63 – 73 yrs vs. younger groups 13-17, 19-27 or 40-58), but suggests that the results could be confounded by enhanced activation of the middle-ear muscle reflex in the older group (Abdala et al., 2014).

Thus, an age-related decline in MOC innervation density, especially in the high-frequency regions where energy from many consonants is concentrated, could also contribute to the reduced hearing-in-noise abilities that are a classic feature of age-related hearing loss. However, equally important to any age-related performance decrements is the loss of the OHCs themselves, without which the MOC system is unable to perform any adjustment of the dynamic range.

Acknowledgements

The assistance of Diane Jones in temporal-bone removal is gratefully acknowledged. The rhesus cochlear tissue was obtained courtesy of Drs. Troy Hackett and Ram Ramachandran from the Department of Speech and Hearing Sciences at Vanderbilt University. Research supported by the Lauer Tinnitus Center and by grants from the NIDCD (P50 015857 and R01 DC 00188).

References Cited

Abdala C, Dhar S, Ahmadi M, Luo P (2014) Aging of the medial olivocochlear reflex and associations with speech perception. J Acoust Soc Am 135:754-765.

Backus BC, Guinan JJ, Jr. (2006) Time-course of the human medial olivocochlear reflex. J Acoust Soc Am 119:2889-2904.

Boyev KP, Liberman MC, Brown MC (2002) Effects of anesthesia on efferent-mediated adaptation of the DPOAE. J Assoc Res Otolaryngol 3:362-373.

Burgess BJ, Adams JC, Nadol JB, Jr. (1997) Morphologic evidence for innervation of Deiters' and Hensen's cells in the guinea pig. Hear Res 108:74-82.

Chambers AR, Hancock KE, Maison SF, Liberman MC, Polley DB (2012) Sound-evoked olivocochlear activation in unanesthetized mice. J Assoc Res Otolaryngol 13:209-217.

Collet L, Kemp DT, Veuillet E, Duclaux R, Moulin A, Morgon A (1990) Effect of contralateral auditory stimuli on active cochlear micro-mechanical properties in human subjects. Hear Res 43:251-262.

Darrow KN, Maison SF, Liberman MC (2006) Cochlear efferent feedback balances interaural sensitivity. Nat Neurosci 9:1474-1476.

Darrow KN, Maison SF, Liberman MC (2007) Selective removal of lateral olivocochlear efferents increases vulnerability to acute acoustic injury. J Neurophysiol 97:1775-1785.

Delgutte B (1990) Physiological mechanisms of psychophysical masking: observations from auditory-nerve fibers. J Acoust Soc Am 87:791-809.

Fuchs PA, Lauer AM (2019) Efferent Inhibition of the Cochlea. Cold Spring Harb Perspect Med 9.

Giraud AL, Garnier S, Micheyl C, Lina G, Chays A, Chery-Croze S (1997) Auditory efferents involved in speech-in-noise intelligibility. Neuroreport 8:1779-1783.

Gordon-Salant S (2005) Hearing loss and aging: new research findings and clinical implications. J Rehabil Res Dev 42:9-24.

435 Greenwood DD (1990) A cochlear frequency-position function for several species--29 years later. J
436 Acoust Soc Am 87:2592-2605.

437 Groff JA, Liberman MC (2003) Modulation of cochlear afferent response by the lateral olivocochlear
438 system: activation via electrical stimulation of the inferior colliculus. J Neurophysiol 90:3178-
439 3200.

440 Guinan JJ, Jr. (2010) Cochlear efferent innervation and function. Curr Opin Otolaryngol Head Neck Surg
441 18:447-453.

442 Guinan JJ, Jr., Gifford ML (1988) Effects of electrical stimulation of efferent olivocochlear neurons on
443 cat auditory-nerve fibers. III. Tuning curves and thresholds at CF. Hear Res 37:29-45.

444 Guinan JJ, Jr., Warr WB, Norris BE (1983) Differential olivocochlear projections from lateral versus
445 medial zones of the superior olivary complex. Journal of Comparative Neurology 221:358-370.

446 Guinan JJ, Jr., Warr WB, Norris BE (1984) Topographic organization of the olivocochlear projections
447 from the lateral and medial zones of the superior olivary complex. J Comp Neurol 226:21-27.

448 Irving S, Moore DR, Liberman MC, Sumner CJ (2011) Olivocochlear efferent control in sound
449 localization and experience-dependent learning. J Neurosci 31:2493-2501.

450 Ishii T, Murakami Y, Balogh K, Jr. (1967) Acetylcholinesterase activity in the efferent nerve fibers of the
451 human inner ear. Ann Otol Rhinol Laryngol 76:69-82.

452 Jacobson M, Kim S, Romney J, Zhu X, Frisina RD (2003) Contralateral suppression of distortion-product
453 otoacoustic emissions declines with age: a comparison of findings in CBA mice with human
454 listeners. Laryngoscope 113:1707-1713.

455 Johnson DH (1980) The relationship between spike rate and synchrony in responses of auditory-nerve
456 fibers to single tones. J Acoust Soc Am 68:1115-1122.

457 Kawase T, Delgutte B, Liberman MC (1993) Antimasking effects of the olivocochlear reflex. II.
458 Enhancement of auditory-nerve response to masked tones. J Neurophysiol 70:2533-2549.

459 Kim S, Frisina DR, Frisina RD (2002) Effects of age on contralateral suppression of distortion product
460 otoacoustic emissions in human listeners with normal hearing. Audiol Neurootol 7:348-357.

461 Klinke R, Galley N (1974) Efferent innervation of vestibular and auditory receptors. Physiol Rev 54:316-
462 357.

463 Konomi U, Kanotra S, James AL, Harrison RV (2014) Age related changes to the dynamics of
464 contralateral DPOAE suppression in human subjects. J Otolaryngol Head Neck Surg 43:15.

465 Kujawa SG, Liberman MC (1997) Conditioning-related protection from acoustic injury: effects of chronic
466 deefferentation and sham surgery. J Neurophysiol 78:3095-3106.

467 Liberman MC (1980) Efferent synapses in the inner hair cell area of the cat cochlea: An electron
468 microscopic study of serial sections. Hear Res 3:189-204.

469 Liberman MC (1988) Response properties of cochlear efferent neurons: monaural vs. binaural stimulation
470 and the effects of noise. J Neurophysiol 60:1779-1798.

471 Liberman MC (1989) Rapid assessment of sound-evoked olivocochlear feedback: suppression of
472 compound action potentials by contralateral sound. Hear Res 38:47-56.

473 Liberman MC (1991) The olivocochlear efferent bundle and susceptibility of the inner ear to acoustic
474 injury. J Neurophysiol 65:123-132.

475 Liberman MC, Brown MC (1986) Physiology and anatomy of single olivocochlear neurons in the cat.
476 Hear Res 24:17-36.

477 Liberman MC, Gao WY (1995) Chronic cochlear de-efferentation and susceptibility to permanent
478 acoustic injury. Hear Res 90:158-168.

479 Liberman MC, Dodds LW, Pierce S (1990) Afferent and efferent innervation of the cat cochlea:
480 quantitative analysis with light and electron microscopy. J Comp Neurol 301:443-460.

481 Liberman MC, Liberman LD, Maison SF (2014) Efferent feedback slows cochlear aging. J Neurosci
482 34:4599-4607.

483 Liberman MC, O'Grady DF, Dodds LW, McGee J, Walsh EJ (2000) Afferent innervation of outer and
484 inner hair cells is normal in neonatally de-efferented cats. J Comp Neurol 423:132-139.

485 Lilaonitkul W, Guinan JJ, Jr. (2012) Frequency tuning of medial-olivocochlear-efferent acoustic reflexes
486 in humans as functions of probe frequency. J Neurophysiol 107:1598-1611.

487 Lisowska G, Namyslowski G, Orecka B, Misiolek M (2014) Influence of aging on medial olivocochlear
488 system function. Clin Interv Aging 9:901-914.

489 Maison SF, Adams JC, Liberman MC (2003) Olivocochlear innervation in the mouse:
490 immunocytochemical maps, crossed versus uncrossed contributions, and transmitter
491 colocalization. J Comp Neurol 455:406-416.

492 Moore JK, Simmons DD, Guan Y (1999) The human olivocochlear system: organization and
493 development. Audiol Neurootol 4:311-325.

494 Nadol JB (1983a) Serial section reconstruction of the neural poles of hair cells in the human organ of
495 corti. II. Outer hair cells. The Laryngoscope 93:780-791.

496 Nadol JB, Jr. (1983b) Serial section reconstruction of the neural poles of hair cells in the human organ of
497 corti. I. Inner hair cells. Laryngoscope 93:599-614.

498 Nomura Y (1976) Nerve fibers in the human organ of Corti. Acta Otolaryngol 82:317-324.

499 Rajan R (1988) Effect of electrical stimulation of the crossed olivocochlear bundle on temporary
500 threshold shifts in auditory sensitivity. I. Dependence on electrical stimulation parameters. J
501 Neurophysiol 60:549-568.

502 Russell IJ, Muragasu E (1997) Medial efferent inhibition suppresses basilar membrane responses to near
503 characteristic frequency tones of moderate to high intensities. J Acoust Soc Amer 102:1734-1738.

504 Schrott-Fischer A, Egg G, Kong WJ, Renard N, Eybalin M (1994) Immunocytochemical detection of
505 choline acetyltransferase in the human organ of Corti. Hear Res 78:149-157.

506 Schrott-Fischer A, Kammen-Jolly K, Scholtz A, Rask-Andersen H, Glueckert R, Eybalin M (2007)
507 Efferent neurotransmitters in the human cochlea and vestibule. Acta Otolaryngol 127:13-19.

508 Schuknecht HF (1993) Pathology of the Ear, 2nd Edition. Baltimore: Lea & Febiger.

509 Spoendlin H (1975) Retrograde degeneration of the cochlear nerve. Acta Otolaryngol 79:266-275.

510 Spoendlin H (1979) Neural connections of the outer haircell system. Acta Otolaryngol 87:381-387.

511 Suthakar K, Ryugo DK (2017) Descending projections from the inferior colliculus to medial
512 olivocochlear efferents: Mice with normal hearing, early onset hearing loss, and congenital
513 deafness. Hear Res 343:34-49.

514 Taberner AM, Liberman MC (2005) Response properties of single auditory nerve fibers in the mouse. J
515 Neurophysiol 93:557-569.

516 Thiers FA, Burgess BJ, Nadol JB, Jr. (2002) Axodendritic and dendrodendritic synapses within outer
517 spiral bundles in a human. Hear Res 164:97-104.

518 Tsuji J, Liberman MC (1997) Intracellular labeling of auditory nerve fibers in guinea pig: central and
519 peripheral projections. J Comp Neurol 381:188-202.

520 Valero MD, Burton JA, Hauser SN, Hackett TA, Ramachandran R, Liberman MC (2017) Noise-induced
521 cochlear synaptopathy in rhesus monkeys (Macaca mulatta). Hear Res 353:213-223.

522 Walsh EJ, McGee J, McFadden SL, Liberman MC (1998) Long-term effects of sectioning the
523 olivocochlear bundle in neonatal cats. J Neurosci 18:3859-3869.

524 Warren EH, 3rd, Liberman MC (1989) Effects of contralateral sound on auditory-nerve responses. I.
525 Contributions of cochlear efferents. Hear Res 37:89-104.

526 Wiederhold ML, Kiang NY (1970) Effects of electric stimulation of the crossed olivocochlear bundle on
527 single auditory-nerve fibers in the cat. J Acoust Soc Am 48:950-965.

528 Winslow RL, Sachs MB (1987) Effect of electrical stimulation of the crossed olivocochlear bundle on
529 auditory nerve response to tones in noise. J Neurophysiol 57:1002-1021.

530 Wu PZ, Liberman LD, Bennett K, de Gruttola V, O'Malley JT, Liberman MC (2018) Primary Neural
531 Degeneration in the Human Cochlea: Evidence for Hidden Hearing Loss in the Aging Ear.
532 Neuroscience.

533 Yin Y, Liberman LD, Maison SF, Liberman MC (2014) Olivocochlear innervation maintains the normal
534 modiolar-pillar and habenular-cuticular gradients in cochlear synaptic morphology. J Assoc Res
535 Otolaryngol 15:571-583.

536

Figures and Captions

Figure 1: Schematic illustration of the organ of Corti showing the afferent and efferent innervation of the inner hair cells (IHCs) and outer hair cells (OHCs), including both the lateral (L) and medial (M) divisions of the olivocochlear (OC) feedback system. Efferents in the IHC area spiral in two bundles, the inner spiral bundle (ISB) and the tunnel spiral bundle (TSB), while afferents underneath the OHCs spiral in the outer spiral bundles (OSBs).

Figure 2: Patterns of hair cell loss in the 23 human temporal bones analyzed in the present study. **A:** Age-related loss of hair cells, showing mean survival in each case, averaged over the 11 half-octave samples within the audiometric frequency range (0.25 – 8.0 kHz inclusive). OHC values represent the average of all three rows. Best-fit straight lines are shown in red as indicated in the key, along with correlation coefficients and p values. **B,C**: Frequency pattern of hair cell loss, showing mean survival (±SEMs) of IHCs (**B**) and OHCs (**C**) at each of the 14 half-octave cochlear-frequency locations sampled. Cases are arbitrarily divided into three age groups, as illustrated in **A**. Significance of the intergroup differences are indicated by asterisks: *$p < 0.05$; **$p < 0.005$; ***$p < 0.0005$; ****$p < 0.0001$

Figure 3: Most of the ChAT-positive fibers in the osseous spiral lamina (OSL) are unmyelinated. These images from two confocal z-stacks are both from a 78 yr old male. In each cochlear frequency region (**A** – 0.35 kHz; **B** – 4.0 kHz) a maximum projection in the xy plane is shown, along with a selected xz and zy slice, positioned as indicated by the dashed yellow lines. Black-filled arrowheads in both xy projections point to the spiraling bundles of efferent fibers. Arrowhead in **Azy** points to a spiraling myelinated efferent (ChAT-positive) axon, while the arrowhead in **Axz** points to the unmyelinated radially directed portion of an efferent axon. Scale bar and orientation arrows in **B** apply to **A**. X arrows point along the spiral towards the base, y arrows point radially towards the organ of Corti, and z arrows point towards scala tympani.

Figure 4: Confocal images of the MOC innervation of OHCs in a middle-aged (**A,B**) vs. an older (**C,D**) subject. From each subject, two views of the same confocal z-stack are shown: **B** and **D** are maximum projections in the acquisition (xy) plane, while **A** and **C** are maximum projections of the entire stacks in the zy plane, i.e. rotated 90º to show the view along the axis of the cochlear spiral, with the approximate boundaries of the three OHC rows indicated in white dashed lines. White arrowheads in **A** and **C** point to MOC terminals at the bases, or along the sides of OHCs, while black-filled arrowheads point to MOC terminals within the spiraling bundles of type-II fibers (e.g. at the arrowheads in **B** and **D**). Immunostaining key and scale bar in **C** apply to all panels. Orientation arrows in **A** and **B** apply to **C** and **D**, respectively. The x arrows point along the spiral towards the apex, y arrows point radially away from the modiolus, and z arrows point towards scala tympani. Dashed yellow boxes enclose the regions included in the digitizations used to quantify MOC terminal density without including tunnel-crossing fascicles.

Figure 5: MOC innervation density decreases significantly with age. **A**: Each point shows the mean area of the ChAT-positive boutons in the OHC area, averaged over 11 half-octave samples within the audiometric frequency range (0.25 – 8.0 kHz inclusive) in each case. The correlation coefficient for the linear regression is shown along with the p value. **B,C**: Frequency pattern of MOC innervation density, showing mean values (±SEMs), for cases arbitrarily divided into three age groups, as shown by the grey boxes in **A**. In all panels, MOC area is expressed in kilopixels, as extracted from maximum projections in the xy plane, such as those in Figures 4B and 4D. The data in **C** are the same as those in **B**, except they have been normalized by dividing by the number of surviving OHCs in the same z-stack. Significance of the intergroup differences are indicated by asterisks as described for Figure 2: precise p values are in the text.

Figure 6: Confocal images of the LOC innervation of IHCs from the apical (**A,B**) vs. basal (**C,D**) half of the cochlea from one subject. At each locus, two views of the same confocal z-stack are shown: **B** and **D** are maximum projections in the acquisition plane (xy), while **A** and **C** are maximum projections of the entire stacks in the zy plane, with the approximate boundaries of the IHCs indicated in white dashed lines. White-filled arrowhead in all panels point to ChAT-positive boutons in the inner spiral bundle (ISB), while the black-filled arrowhead in **B** points to a ChAT positive bouton in the tunnel spiral bundle (TSB). Immunostaining key and scale bar in **D** apply to all panels, and the orientation arrows in **C** and **D** also apply to **A** and B, respectively: the x arrows point along the spiral towards the apex, y arrows point radially away from the modiolus, and z arrows point towards scala tympani.

Figure 7: LOC innervation density decreases with age, but not after correction for the loss of IHCs. **A**: Each point shows the mean area of the ChAT-positive boutons in the IHC area, averaged over 11 half-octave samples within the audiometric frequency range (0.25 – 8.0 kHz inclusive) in each case. The correlation coefficient and p value for the linear regression is shown. **B**: Frequency pattern of LOC area measures, showing mean values (±SEMs), for cases arbitrarily divided into three age groups, as shown by the grey boxes in **A**. **C**: Same data as in B, except the areas have been divided by the number of surviving IHCs in the same z-stacks. In all panels, LOC area is expressed in kilopixels, as extracted from maximum projections in the xy plane, such as those in Figures 3B and 2D. The ChAT immunostaining in LOC area for the youngest subject (0.1 yrs) was too dim and indistinct to be reliably measured. Significance of the intergroup differences are indicated by asterisks as described in Figure 2: precise p values are in the text.

Figure 8: In humans, the MOC innervation is less dense than in other mammals. Each micrograph is the maximum projection from the ChAT channel of a z-stack taken from the cochlear region of maximum innervation density in each of four species: human (4.0 kHz region of a 39-yr old female), rhesus macaque (2.0 kHz region of a 9 yr-old male), guinea pig (4.0 kHz region of a 1.5 month-old female) and mouse (22.6 kHz region of a 1.5 month-old male). In each image, locations of the three OHC rows are indicated, and the outlines of the 1st-row OHCs (cuticular plates) are schematized (to scale, but regularized and offset vertically for clarity) as extracted from the same z-stack. In each image, tunnel-crossing efferent bundles are noted by arrowheads: in the mouse image, the tunnel crossing bundles are truncated, because the original image field was more restricted than the others. Scale bar in the human panel applies to all images.

Figure 9: Quantification of MOC terminal area relative to OHC surface area in each of four species. **A**: The human data are from the middle-aged group in Figure 5, expressed relative to OHC surface areas extracted from the myosin-immunostaining channel in the same image stacks. Mouse, guinea pig and rhesus data are from four ears in each species, immunostained, imaged and analyzed exactly as for the human data and similarly expressed relative to the OHC surface areas extracted from the same set of image stacks. **B**: To demonstrate the functional validity of the MOC silhouette-area metric, we re-analyzed image stacks from a prior study in which MOC feedback strength was measured after partial sectioning of the MOC bundle (Liberman et al., 2014). Each point represents a different case, comparing shock-evoked MOC suppression at the frequency region of maximal effect (22.6 kHz) with the MOC silhouette area in the appropriate cochlear region. The correlation was highly significant ($p << 0.001$).

Figure 10: LOC innervation density in humans is comparable to that in mouse. Confocal projections from the cochlear region with maximal LOC innervation: 0.35 kHz in human (**A,B**) vs. 8.0 kHz in mouse (**C,D**). The human case was a 59 yr-old female. For each species, two views of the same confocal z-stack are shown: **B** and **D** are maximum projections in the acquisition plane (yx), while **A** and **C** are maximum projections of the entire z-stacks in the yz plane. Orientation arrows in **A** and **B** also apply to **C** and **D**, respectively: x arrows point along the spiral towards the apex, y arrows point radially away from the modiolus, and z arrows point towards scala tympani. White arrowheads in **A** and **B** point to ChAT-positive LOC terminals at the bases of IHCs; black-filled arrowheads in **B** and **D** point to the ChAT-positive tunnel-crossing fibers that give rise to MOC terminals. Red-filled arrowhead in **A** points to IHC

633 cuticular plates, and the rough outline of IHCs is shown as a dashed line. Immunostaining key in **A**
634 applies to all panels. Scale bars in **A** and **C**, apply to **B** and **D**, respectively.

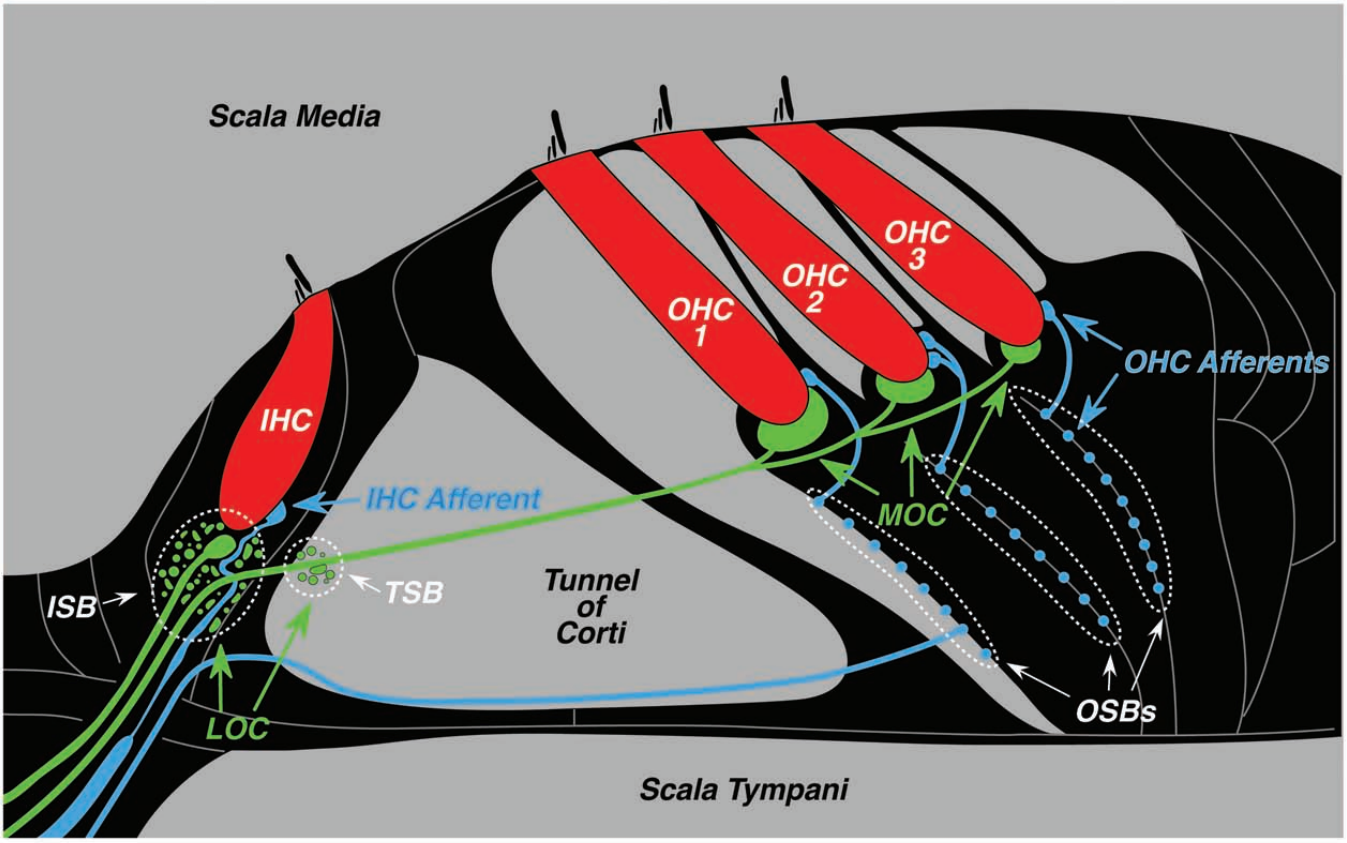

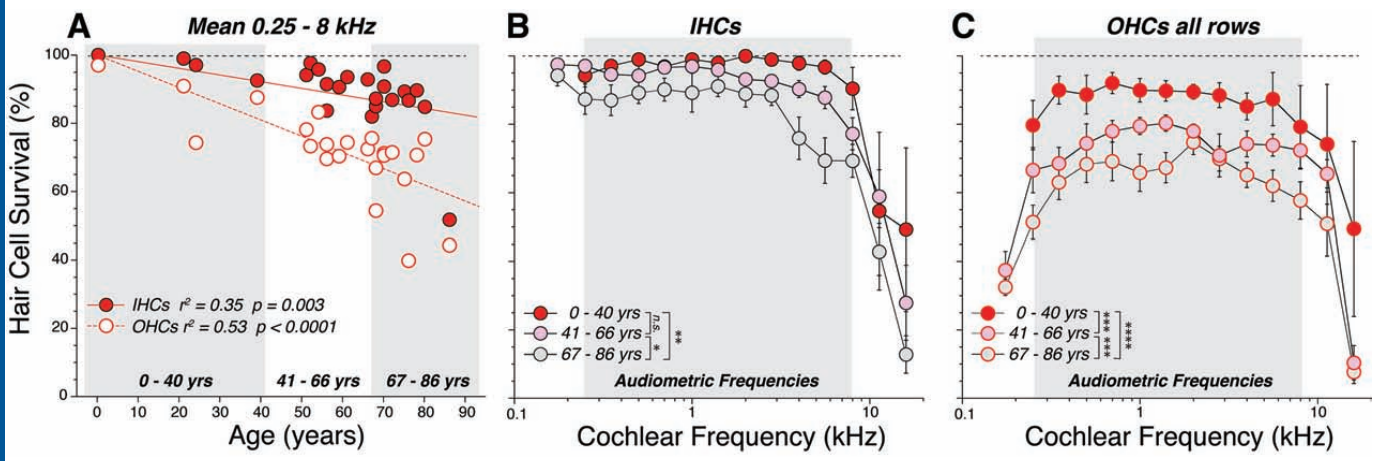

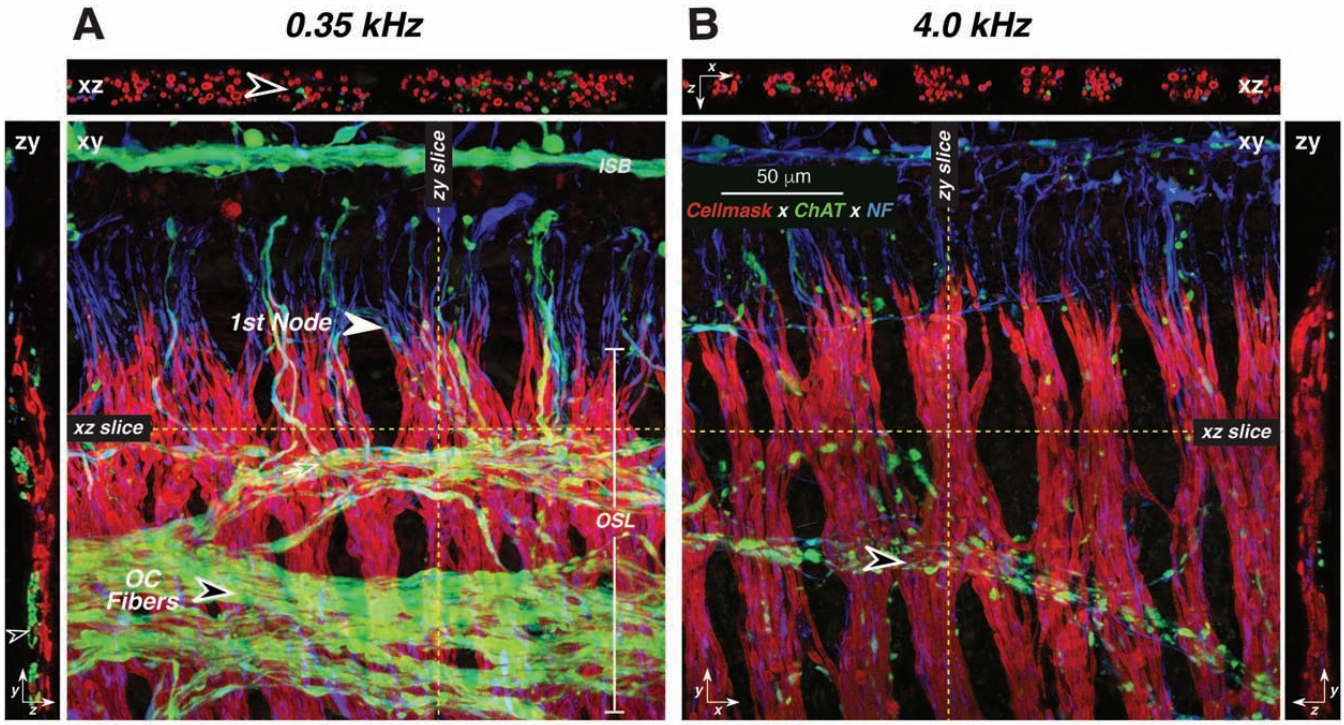

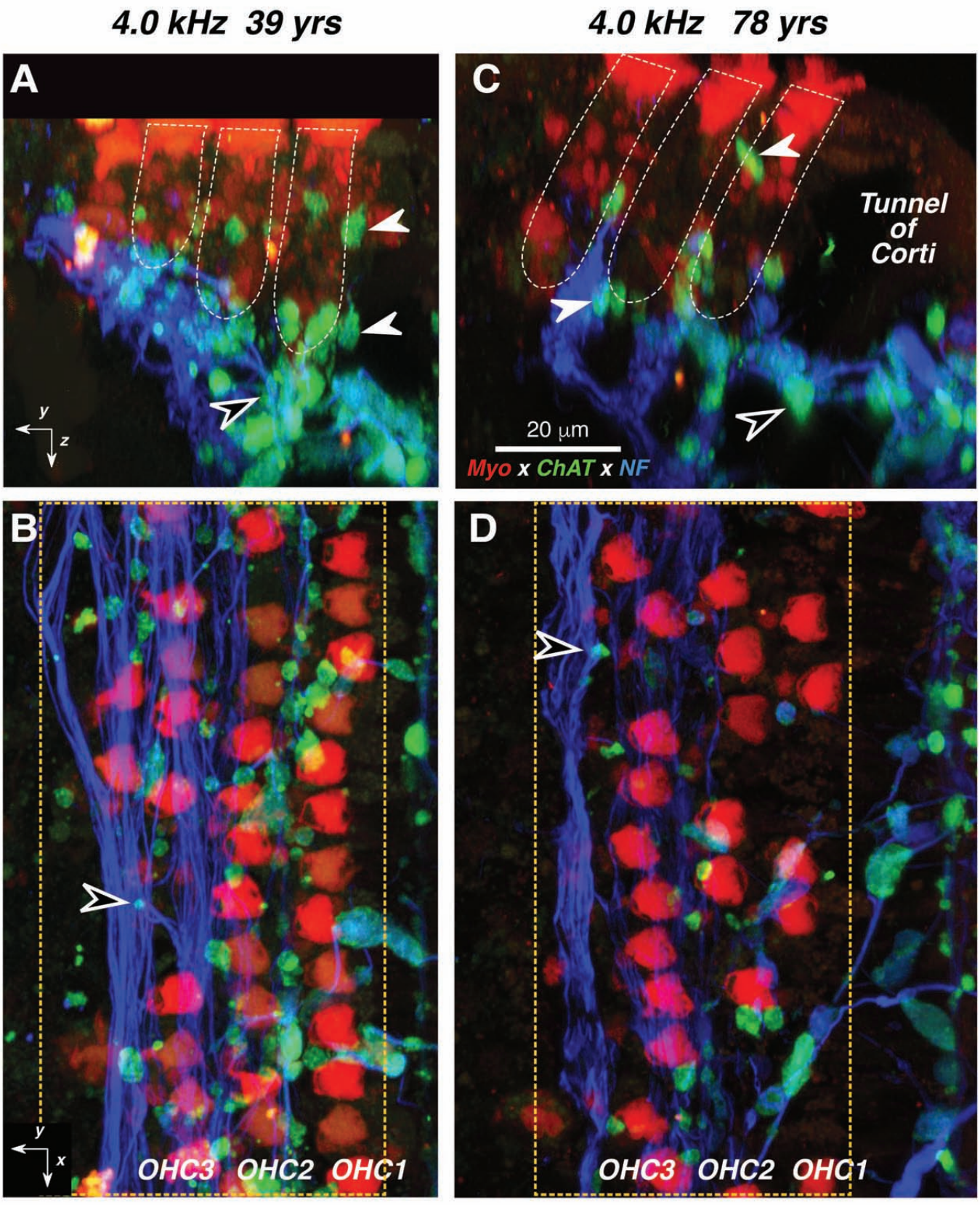

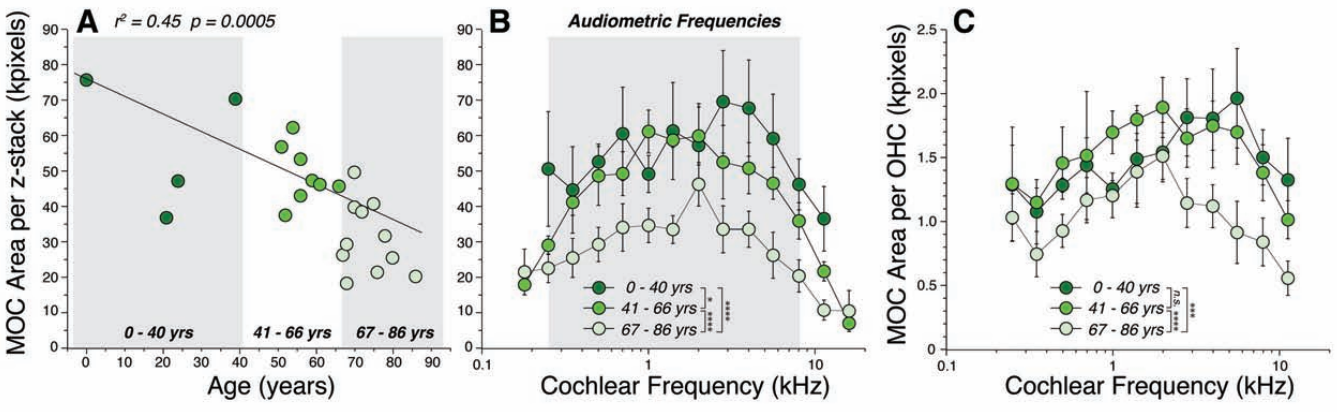

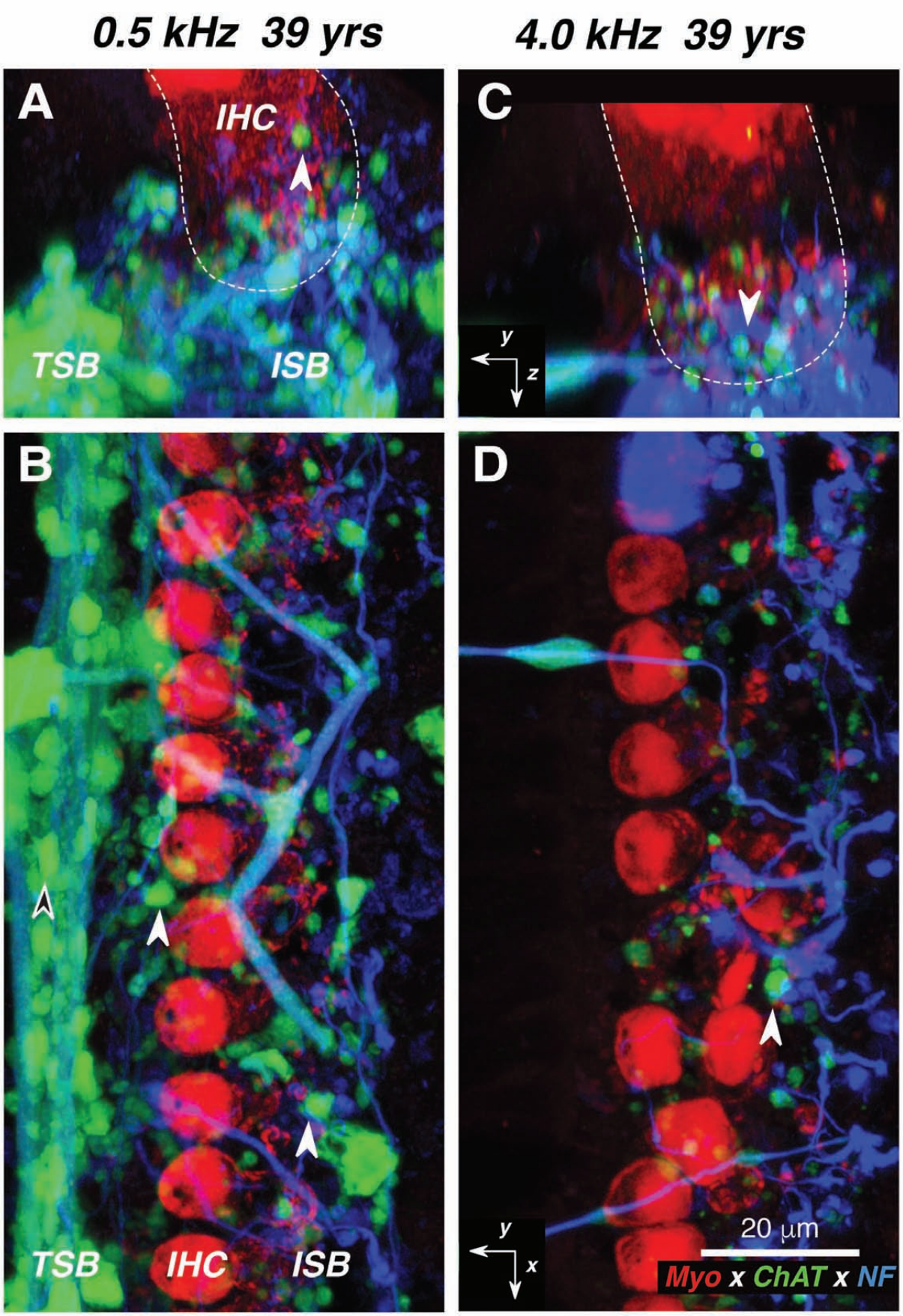

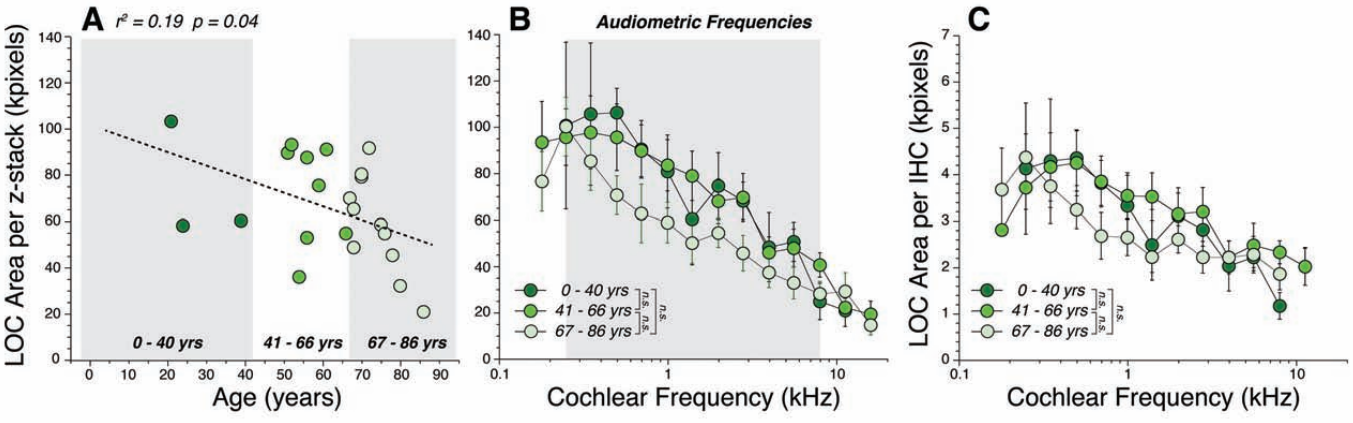

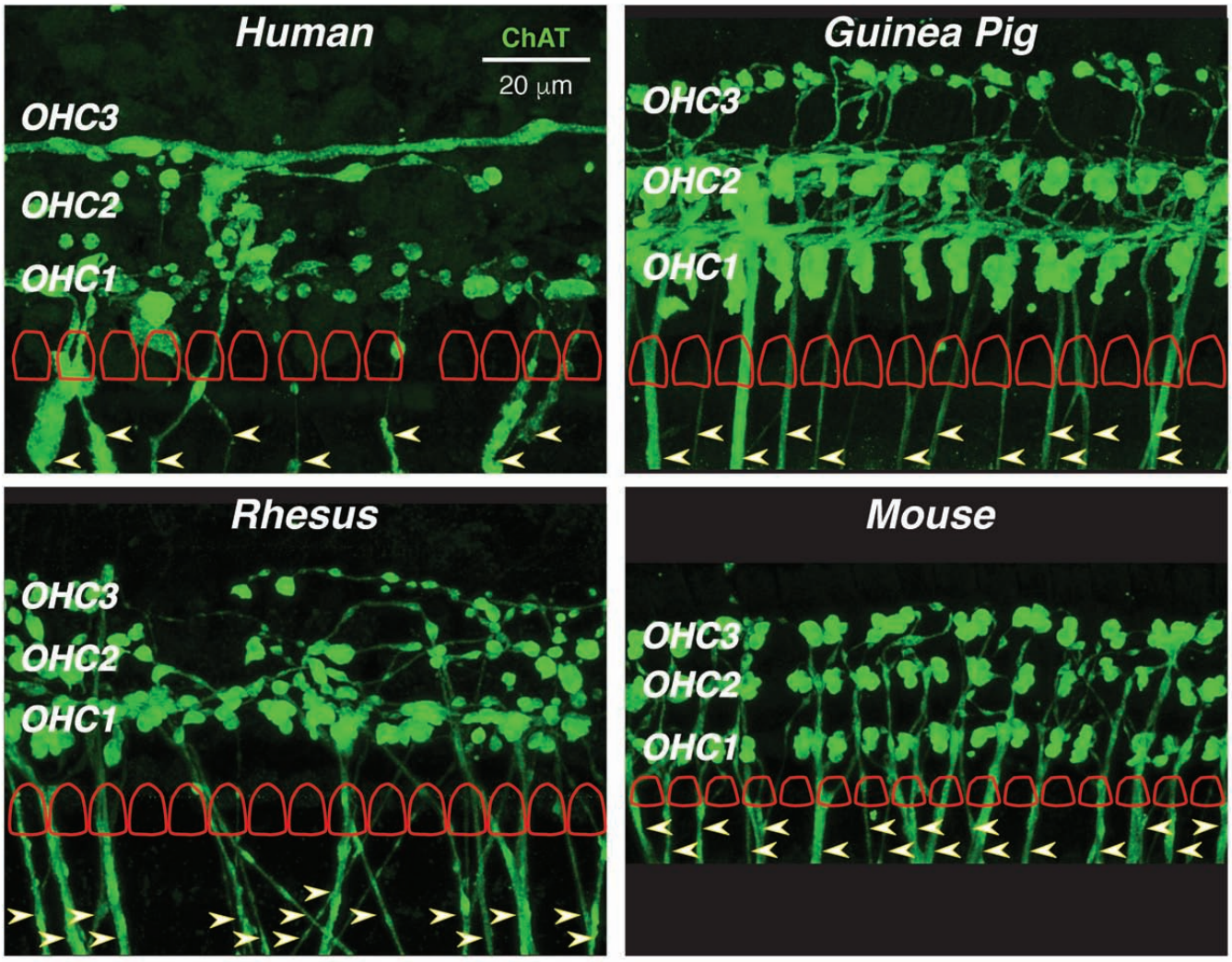

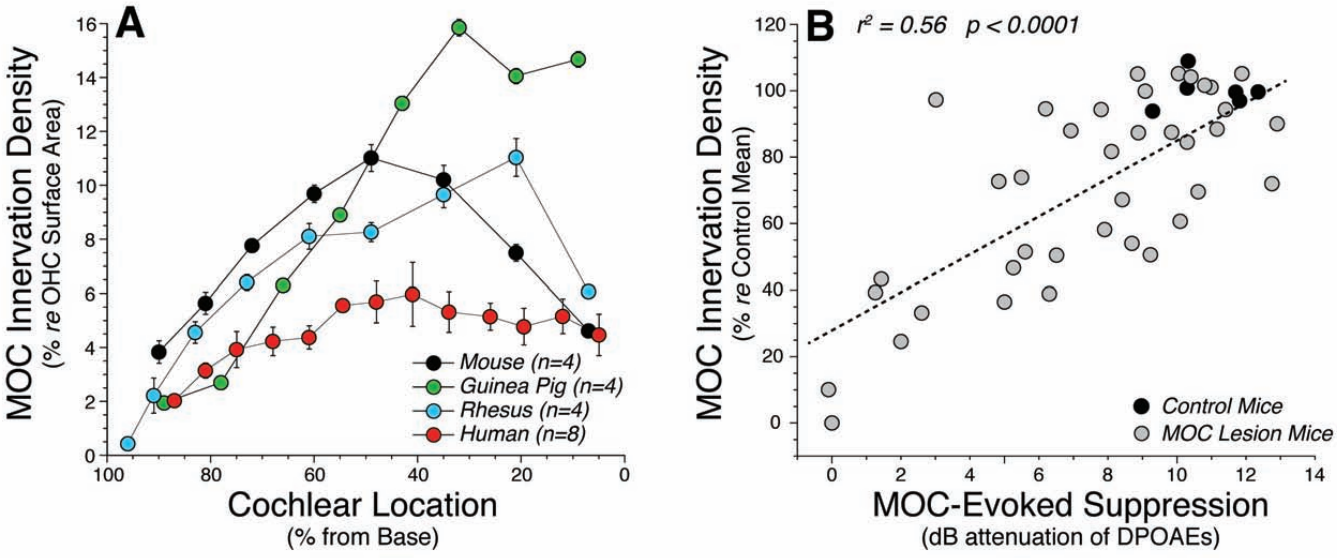

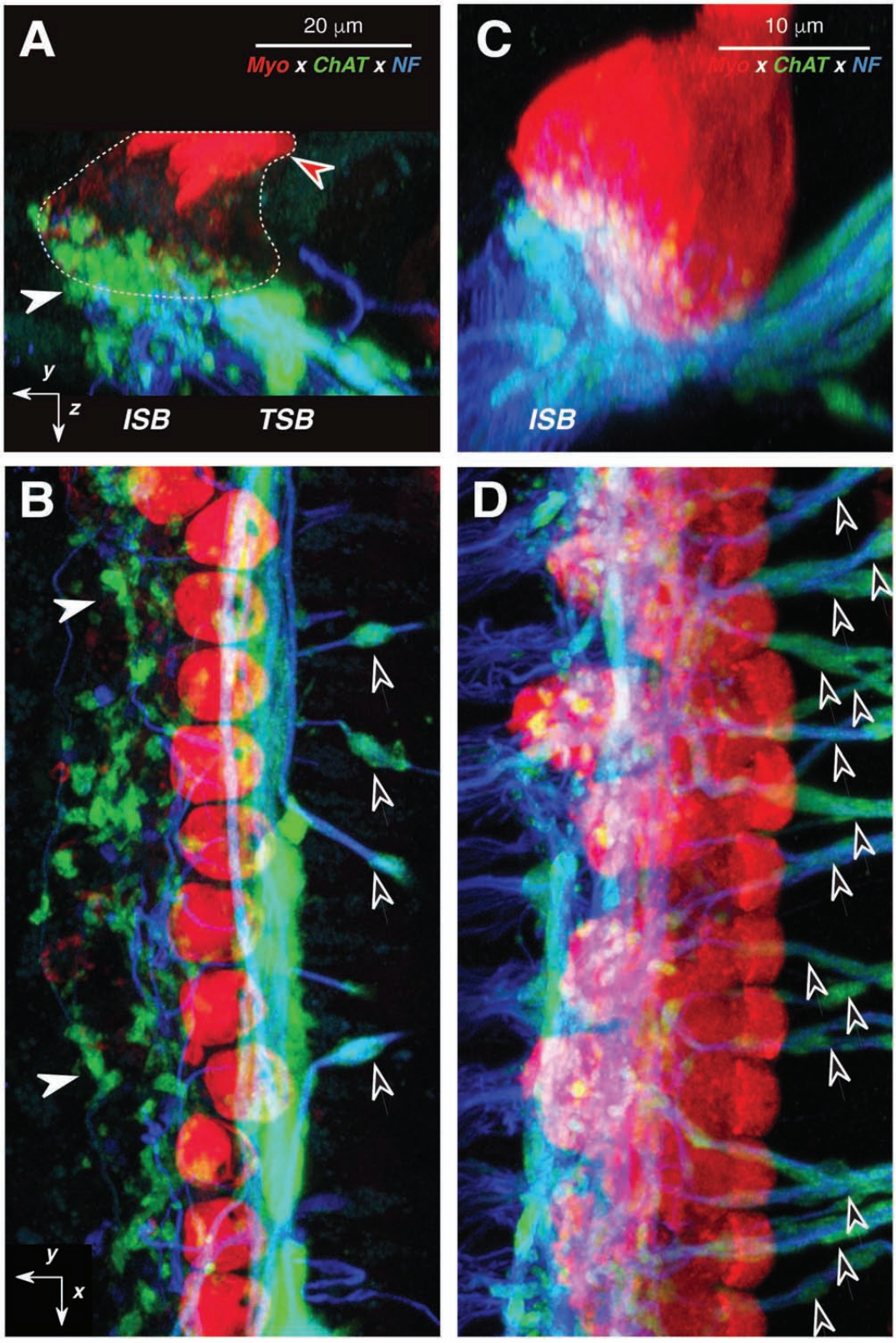

Human 0.35 kHz
~80% locus

Mouse 8.0 kHz
~80% locus